Applied Catalysis A: General 524 (2016) 192–199

Contents lists available at ScienceDirect

Applied Catalysis A: General

journal homepage: www.elsevier.com/locate/apcata

Catalytic properties and nature of active centers of ferrospheres in oxidative coupling of methane

Alexander G. Anshits[a,*], Oleg A. Bayukov[a,b], Evgenii V. Kondratenko[c], Natalia N. Anshits[a], Oleg N. Pletnev[b], Evgenii V. Rabchevskii[a], Leonid A. Solovyov[a]

[a] Institute of Chemistry and Chemical Technology, Siberian Branch of the Russian Academy of Sciences, Akademgorodok 50/24, 660036 Krasnoyarsk, Russia
[b] Kirensky Institute of Physics, Siberian Branch of the Russian Academy of Sciences, Akademgorodok 50/38, 660036 Krasnoyarsk, Russia
[c] Leibniz-Institut für Katalyse e.V. an der Universität Rostock, Albert-Einstein-Str. 29 a, D-18059 Rostock, Germany

ARTICLE INFO

Article history:
Received 11 March 2016
Received in revised form 31 May 2016
Accepted 21 June 2016
Available online 22 June 2016

Keywords:
Methane coupling
Active center
Ferrospinel
Mössbauer spectroscopy

ABSTRACT

Ferrospheres with the Fe_2O_3 content in the range from 76 to 97 wt% were applied as catalysts for the oxidative coupling of methane (OCM). To identify their phase composition and distribution of iron sites, the ferrospheres were characterized by X-ray powder diffraction and Mössbauer spectroscopy before and after the OCM reaction. Magnetite-based ferrite spinel, hematite and aluminosilicate glasses were established to be the main phases. The ferrospinel of all ferrospheres partially oxidized to hematite after the OCM reaction. It was established that the yield of C_2-hydrocarbons sharply increased at the ferrospheres with Fe_2O_3 content higher than 89 wt% The spinel phase of these ferrospheres includes Fe^{vv3+}(B) sites with a Ca^{2+} tetrahedral cation and an octahedral cation vacancy among the nearest neighbors. A linear correlation between the yield of C_2-hydrocarbons (ethane and ethylene) and the content of such sites was established, thus indicating that their electrophilic oxygen species participate in selective CH_4 conversion to C_2H_6.

1. Introduction

The oxidative coupling of methane (OCM) is a promising way for the direct conversion of the most inert hydrocarbon, i.e. methane, into C_2-hydrocarbons (ethylene and ethane). Over a period of more than 30 years, a large number of different catalytic materials have been tested for this reaction [1–9]. Unfortunately, all known OCM catalysts suffer from insufficiently high selectivity to C_2-hydrocarbons for industrially relevant (>30%) degrees of methane conversion. This is due to the fact, that the desired hydrocarbons are easily oxidized to CO and CO_2 because they are more reactive than methane. As a consequence, kinetic studies predict a limit for the maximal yield of C_2-hydrocarbons [7,10,11], which is around 28 or 30% when performing the OCM reaction with co-feeding [10] or alternating feeding [11] of CH_4 and O_2, respectively. Based on this background, improvements in the OCM performance may be achieved by kinetic controlling selective (formation of C_2-hydrocarbons) and non-selective (combustion of hydrocarbons) reaction pathways, which are influenced by various physico-chemical properties of the catalysts applied. Therefore, one of possible approaches for developing novel selective catalytic materials is to establish fundamental relationships between their selectivity/activity and physico-chemical properties as detail as possible.

As shown in our previous studies [12,13], ferrospheres separated from fly ashes produced upon combustion of high-calcium brown coals are promising OCM catalysts with catalytically active Ca-promoted ferrospinel phase. Their OCM performance is strongly influenced by the iron content. Ferrospheres possessing 87.5 wt% Fe_2O_3 and etched by an aqueous solution of HF showed the selectivity to C_2-hydrocarbons of 70% at the methane conversion of 24% at 850 °C [13]. Contrarily, ferrospheres and magnetic cenospheres with a lower iron content oxidized methane to carbon oxides [14,15]. In order to elucidate possible fundamental reasons for the different OCM performance, we thoroughly characterized ferrospheres with the content of Fe_2O_3 in the range of 30–92 wt% to determine their composition, morphology, microstructure of iron-containing phases, and catalytic properties [16–18]. In particular, it was demonstrated that the aluminum-magnesium-ferrite spinel is the main phase in ferrospheres with the content of Fe_2O_3 lower than 80 wt% and high concentration of SiO_2 and Al_2O_3. For those with a higher Fe_2O_3 content (>85 wt%), the CaO-promoted

* Corresponding author.
E-mail address: anshits@icct.ru (A.G. Anshits).

http://dx.doi.org/10.1016/j.apcata.2016.06.032
0926-860X/

ferrite spinel and the hematite phases were identified. The former had the unit cell parameter exceeding the corresponding parameter of stoichiometric magnetite, while the latter had the unit cell parameters close to those of stoichiometric α-$Fe_2O_3$1 [6,17]. According to our previous study [18], the ferrospheres with the aluminum–magnesium–ferrite spinel are not selective OCM catalysts, yielding CO_x mainly. This undesired reaction on the ferrospheres containing the calcium ferrite spinel is suppressed in favor of C_2-hydrocarbons formation.

Based on the above background, the objective of this work is to establish relationships between the phase composition, microstructure of the ferrospinel phase, the state and distribution of iron within the crystallographic sites of the iron-containing phases in differently composed ferrospheres and their OCM performance. In particular, we focus on gaining insights into possible catalytic sites responsible for selective and non-selective methane oxidation. To this end, fresh and used (after the OCM reaction) catalysts were characterized by Mössbauer spectroscopy and the obtained spectra were rigorously evaluated. Steady-state catalytic tests were performed at 750 and 825 °C.

2. Experimental

2.1. Catalytic materials

Eleven narrow fractions of high-calcium ferrospheres with Fe_2O_3 content 76–97 wt% were used as catalytic materials for the oxidative coupling of methane. The samples are labeled as B(n), S(n), and SMF(n), where B, S is the source of fly ash from which the ferrospheres were separated and (n) is the weight percentage of Fe_2O_3. The ferrospheres of series B(n) and S(n) were separated from ferrisialic type fly ash from combustion of coal Tugnuisky Deposit (Buryatia) and the calsialic type fly ash from combustion of coal Berezovsky Deposit (Krasnoyarsk region), respectively. The chemical and phase composition, morphology of the globules, and microstructural characteristics of the initial B and S series were studied in detail in our previous study [16,17]. The ferrospheres of the SMF series were obtained from fractions −0.05 and −0.063 + 0.05 mm of the S series by the grain-size classification and separation in a gradient magnetic field. Table 1 shows the chemical composition of all studied materials and their specific surface areas determined from Ar desorption according to the multipoint Brunauer–Emmett–Teller (BET) method (NOVA 3200e instrument). Fig. 1 exemplarily shows optical and SEM images of selected ferrosphere fractions SMF(91.4) and SMF(93.5). It is important to note that ferrospheres of series B (Table 1) originate from the melt of the system FeO–SiO_2–Al_2O_3, and their chemical composition corresponds to the total regression equations $[SiO_2] = 65.71–0.71[Fe_2O_3]$ with the correlation coefficient r = −0.99 and $[Al_2O_3] = 24.92–0.26[Fe_2O_3]$ with r = −0.97, which are characteristic for this system [16]. Ferrospheres of S and SMF series (Table 1) were formed from the melt of the system FeO—CaO–SiO_2 and their chemical composition is described by two other regression equations $[CaO] = 56.47–0.56[Fe_2O_3]$ and $[SiO_2] = 24.62–0.25[Fe_2O_3]$ with the correlation coefficients r = −0.97 and −0.90, respectively.

2.2. Catalyst tests

Catalytic tests were performed in a continuous-flow fixed-bed quartz tube reactor with inner diameter of 4–8 mm at 750–850 °C and a total pressure of 1.3 at (1at = 98 kPa) using a CH_4:O_2:He = 82:9:9 feed. The amount of the ferrospheres was varied in the range of 0.3–1.3 g, and the contact time (W/F) was 1.2–1.3 g-cat s/ml. The products and feed components were analyzed by an on-line gas chromatograph Agilent 7890A GC equipped with high performance columns «HP Plot Al_2O_3», «Molecular Sieve 5A» and capillary column «DB-1». Experimental errors for determination of methane conversion (X_{CH4}) and selectivity of the product formation (S) in three parallel experiments were 0.25 and 0.5%, respectively.

2.3. X-ray powder diffraction (XRPD) analysis

X-ray powder diffraction (XRPD) analysis using the full-profile Rietveld method [19] and the derivative difference minimization (DDM) [20] was applied for quantifying the phase composition of ferrospheres in their initial (as received) state and after the OCM tests at 750 °C. The former materials have been thoroughly characterized in our previous study [16]. To preserve the catalyst composition formed under the OCM conditions, the catalysts after the catalytic tests at 750 °C were rapidly (~150–200°/min) quenched in the OCM feed before XRPD analysis. X-ray powder diffraction patterns were recorded in the reflection geometry on a PANalytical X'Pert PRO diffractometer (Co Kα radiation, 2Θ scan range 15–115°) equipped with a PIXcel detector. The weight content of X-ray amorphous phase(s) was determined by the external standard method with hematite used as a reference material. The absorption coefficients of the samples for the Co Kα radiation were calculated from the total elemental composition according to the chemical analysis data.

2.4. Mössbauer measurements

Mössbauer spectra of ferrospheres in the initial state and after the OCM tests at 750 °C were recorded on an MS 1104Em gamma-resonance spectrometer with a $^{57}Co(Cr)$ source at room temperature. To preserve the catalyst composition formed under the OCM conditions, the catalysts after catalytic tests at 750 °C were rapidly (~150–200°/min) quenched in the OCM feed before Mössbauer measurements.

Table 1
Chemical composition (wt%) of narrow fractions of ferrospheres used as the catalysts.

Catalyst	Fraction (mm)	Bulk dencity (g/cm^2)	S_{BET} (m^2/g)	SiO_2	Al_2O_3	Fe_2O_3	CaO	MgO	Na_2O	K_2O	TiO_2
B(79.1)	0.063–0.1	1.95	0.38	9.00	6.22	79.12	5.40	0.90	0.23	0.08	0.10
B(76.2)	0.05–0.063	1.99	0.49	9.50	4.64	76.24	9.08	0.81	0.20	0.07	0.19
B(78.4)	<0.05	2.07	0.60	9.41	5.04	78.38	6.24	1.10	0.20	0.05	0.16
S(85.2)	0.2–0.4	1.87	0.33	4.00	1.90	85.20	8.69	1.00	0.25	0.07	0.18
S(88.8)	0.16–0.2	1.93	0.24	2.48	1.20	88.82	7.43	0.81	0.20	0.05	0.19
S(89.8)	0.05–0.063	2.57	0.21	1.35	1.02	89.85	6.70	0.81	0.24	0.10	0.12
S(89.1)	<0.05	2.54	0.34	0.64	0.92	89.12	8.81	0.60	0.10	0.05	0.16
SMF(93.5)	0.032–0.04	2.65	0.19	1.39	0.19	93.51	3.54	0.40	0.29	0.09	<0.01
SMF(91.4)	0.05–0.063	2.46	0.29	1.30	<0.01	91.36	6.57	0.33	0.28	0.06	<0.01
SMF(96.5)	0.05–0.063	2.56	0.20	0.80	<0.01	96.53	3.20	0.08	0.41	0.04	<0.01
SMF(97.2)	0.05–0.063	2.62	0.18	0.36	<0.01	97.25	2.04	0.10	0.28	0.05	<0.01

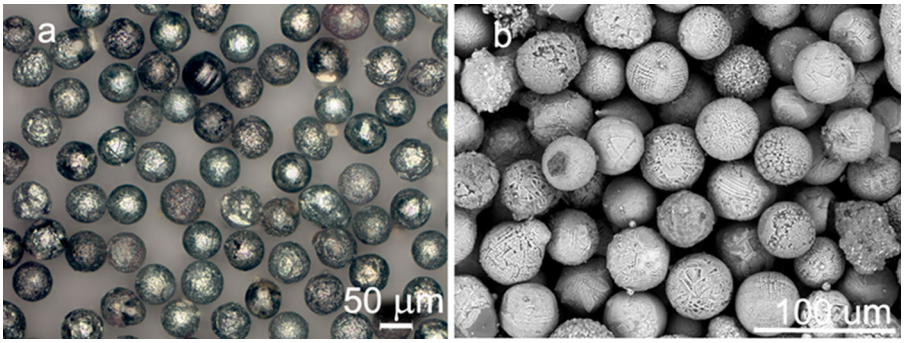

Fig. 1. a) Optical image of ferrospheres SMF(91.4) and b) SEM image of ferrospheres SMF(93.5).

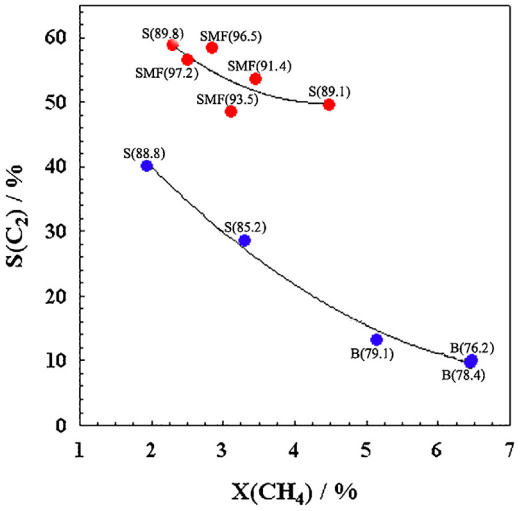

Fig. 2. Selectivity to C_2-hydrocarbons versus CH_4 conversion at 750 °C over ferrospheres with Fe_2O_3 content > 89 wt% ( ) and ferrospheres with Fe_2O_3 content <89 wt% ( ) (reaction feed CH_4:O_2:He = 82:9:9 vol%, contact time (W/F) was 1.2–1.3 g-cat s/ml).

3. Results and discussion

3.1. Catalytic properties of ferrospheres

Selected results of our OCM tests at 750 °C are summarized in Fig. 2 in form of a selectivity–conversion relationship. It should be mentioned that each data point represents a certain catalyst. As seen in this figure, all tested catalysts can be divided into two groups differing in the selectivity to C_2-hydrocarbons and in the effect of CH_4 conversion on the selectivity. For ferrospheres with Fe_2O_3 content of less than 89 wt% (see Table 1 for their detail composition including catalysts abbreviation), the selectivity at the lowest CH_4 conversion of around 2% was below 40–45% and strongly decreased to 10–15% with increasing methane conversion. In comparison with these catalysts, those with Fe_2O_3 content of higher than 89 wt% showed higher (50–72%) selectivity to C_2-hydrocarbons and lower effect of the conversion on the selectivity.

The effect of iron content on OCM performance of ferrospheres is further illustrated in Fig. 3 showing steady-state yields of C_2-hydrocarbons and CO_x obtained at 750 and 825 °C as a function of iron content. For all catalysts, the yield of CO did not exceed 0.8% at both temperatures. Irrespective of the reaction temperature, CO_2 was the main reaction product over the samples with the Fe_2O_3 content lower than 89 wt%. Its yield at 750 °C decreased with increasing Fe_2O_3 content from 76.2 to 88.8 wt%, while no effect was observed at 825 °C. (Fig. 3b). The latter behavior is explained

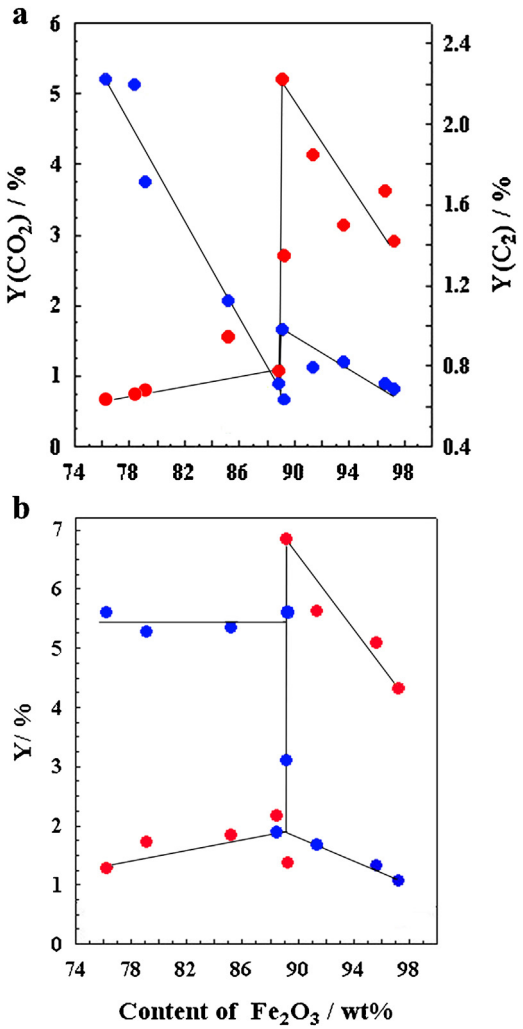

Fig. 3. The effect of Fe_2O_3 content in ferrospheres on the yield of CO_2 ( ) and C_2-hydrocarbons ( ) in the OCM reaction at (a) 750 and (b) 825 °C (reaction feed CH_4:O_2:He = 82:9:9 vol%, contact time (W/F) was 1.2–1.3 g-cat·s/ml).

by the fact that oxygen conversion was complete over all catalysts. Importantly, C_2-hydrocarbons became the main products over the ferrospheres with a Fe_2O_3 content higher than 89%; the yield increased up to 7% at 825 °C. When the iron content increased further, the yield continuously decreased but was always significantly higher than for the materials possessing less than 89 wt% Fe_2O_3. The yield of CO_2 followed an opposite trend. The obtained dependence of OCM performance on Fe_2O_3 content in Fig. 3 strongly suggests an abrupt change between the kinetics of primarily and

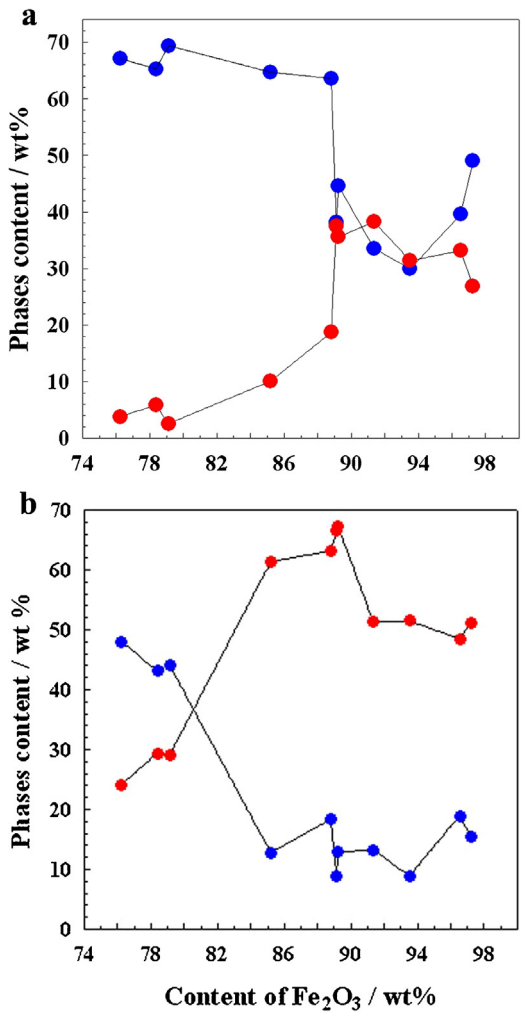

Fig. 4. Weigh percentage of ferrospinel ( ) and hematite ( ) in ferrospheres versus overall Fe_2O_3 content in their (a) initial state and (b) after the OCM reaction at 750 °C.

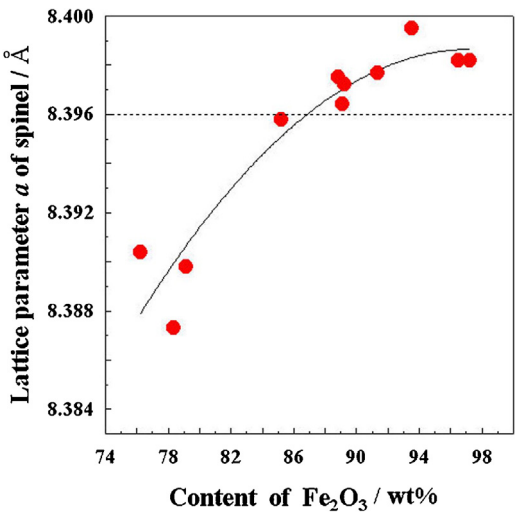

Fig. 5. Effect of Fe_2O_3 content in ferrospheres on lattice parameter of ferrospinel after OCM reaction at 750 °C.

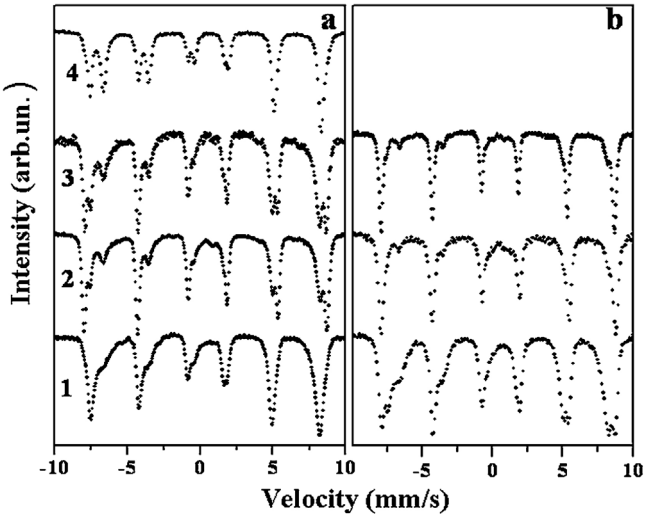

Fig. 6. Selected Mössbauer spectra of ferrospheres fractions 1) B(79.1), 2) S(89.1), 3) SMF(96.5) in initial (a) and steady states (b); 4) spectrum of magnetite.

secondary reaction pathways over ferrospheres with the content of $Fe_2O_3 \geq 89$ wt%.

The phase composition of as-received ferrospheres and those after the OCM reaction is summarized in Fig. 4. One can see that ferrospinel is the dominating phase in the fresh ferrospheres with an overall content of Fe_2O_3 below 89 wt%, while ferrospinel and hematite are present in similar amounts in the ferrospheres with higher Fe_2O_3 content (Fig. 4a). For all ferrospheres, the amount of hematite strongly increased after their use in the OCM reaction at 750 °C. These results suggest that ferrospinel was oxidized to hematite (Fig. 4b). Our quantitative XRPD analysis of these materials also revealed that the lattice parameter of the ferrospinel phase differed from that in the stoichiometric phase and increased with an increase in the overall Fe_2O_3 content in the ferrospheres (Fig. 5). The lattice parameter of spinel exceeds 8.396 Å for most samples possessing more than 89 wt% Fe_2O_3 and showing high OCM performance (Figs. 2 and 3).

Taking into account the present data and our previous characterization results [12,16,18], we suppose that the effect of Fe_2O_3 content in ferrospheres on their OCM performance (Fig. 3) cannot be explained only by their distinctive phase composition and structural parameters of CaO-promoted ferrite spinel and aluminum-magnesium-ferrite spinel. To check if the state and distribution of iron cations influence the catalytic properties, we applied Mössbauer spectroscopy for characterizing the ferrospheres used in the OCM reaction at 750 °C for at least four hours to achieve a steady-state operation. At this temperature, oxygen conversion for samples S(n) and SMF(n) series with Fe_2O_3 content 85–97 wt% (see Table 1 for the abbreviations) changed in the range 9–27% that corresponded to a similar oxygen partial pressure of 0.106–0.085 atm (1 atm = 98 kPa) at the outlet of the reactor in steady-state conditions. This restriction was necessary to exclude any effect of the oxidizing potential of the reaction conditions on the oxidation state and distribution of iron cations in the ferrospinel of ferrospheres in the range of an abrupt change in the pathways of methane conversion (Fig. 2). The obtained results are presented and discussed in the next section.

3.2. State and cation distribution of iron in ferrospheres in the initial and steady states

Fig. 6 shows selected Mössbauer spectra of ferrospheres with different OCM performance in their initial (as received) and steady (after the OCM reaction) states. The interpretation of the spectra was performed in two stages according to the procedure similar to that described in previous studies [21,22]. In the first step, we were aimed at identifying the main iron-containing phases,

i.e. magnetite-based ferrospinel, hematite, and aluminosilicate glass. These results are in agreement with the X-ray diffraction data described and discussed in the preceding section. Hematite was identified by the characteristic parameters of the sextet ($IS \sim 0.38$ mm/s, $H \sim 517$ kOe, and $QS \sim -0.38$ mm/s) [23]. The fast electron exchange of $Fe^{2+} \leftrightarrow Fe^{3+}$ couples designated as $Fe^{2,5+}$, is typical for magnetite. Characteristic Mossbauer parameters of these cations are $IS \sim 0.64$ mm/S and $H \sim 460$ kOe [24]. The paramagnetic parts of the spectrum with very large widths are attributed to the alumosilicate glass ($IS \sim 0.2$–0.5 mm/s, and $QS \sim 0$–2 mm/s) [25].

For the above interpretation of the spectra, we did not consider the complete set of substitutional cations in the spinel phase. Thus, it was not possible to estimate the effect of foreign cations on the state of nonequivalent iron sites, which may influence the OCM performance. To overcome the above limitation, our further analysis was aimed at identifying and describing the positions of iron sites that differ from those in stoichiometric magnetite.

In the spectrum of "stoichiometric" magnetite above the Verwey temperature (~125 K), there are usually two sextets, one of which is attributed to trivalent iron cations located in the tetrahedral sites, i.e., Fe^{3+}(A). The second sextet is assigned to the $Fe^{2.5+}$(B) cations located in the octahedral sites. These sites have the following parameters: $IS = 0.3$ mm/s and $H = 490$ kOe for Fe^{3+}(A), and $IS = 0.66$ mm/s and $H = 460$ kOe for $Fe^{2.5+}$(B). Below the Verwey temperature, to a first approximation there are two sextets, Fe^{3+}(A + B) and Fe^{2+}(B) [26]. The spectra of the sites Fe^{3+}(A) and Fe^{3+}(B) are unresolved. The sites A and B in maghemite γ-Fe_2O_3 are also unresolved [27]. On this basis, the sites designated as Fe^{3+}(A + B) and $Fe^{2.5+}$(B) in ferrospheres were assigned to the sites similar to those in stoichiometric magnetite (Table 2 and Table S1, supplementary data).

In stoichiometric magnetite $Fe_3O_4 \equiv (Fe^{3+})[Fe^{2+}Fe^{3+}]O_4 \equiv (Fe^{3+})[Fe_2{}^{2.5+}]O_4$, the ratio of the number of Fe^{2+} ions to the total number of iron atoms is equal to 0.333, while this ratio in the spinel phase of ferrospheres in their initial and steady states is significantly lower (Fig. S1, supplementary data) and strongly depends on the overall Fe_2O_3 content. This can be associated with both replacement of Fe^{2+} by, for example, Mg^{2+} and/or Ca^{2+} and formation of cation vacancies. Previous experimental results [28–30] suggest that the Ca^{2+} cations in magnetite are located in the tetrahedral sites. The Mg^{2+} cations occupy both types of sites in spinel with a preference for the octahedral sites, while the Al^{3+} cations are located in the octahedral sites at low levels of doping [31].

In addition to the iron sites of stoichiometric magnetite, other iron positions are designated as Fe^{v3+}, $Fe^{v2.5+}$, and Fe^{vv3+} (Table S1, supplementary data). Apparently, the formation of such sites is caused by the imperfection of magnetite. The Mössbauer characteristics of these sites are summarized in Table 2. Fig. 7 shows a fragment of the spinel structure, which explains the appearance of nonequivalent sites in defective magnetite. The assignment of the iron positions in the ferrospinel phase was made by taking into account a certain charge state of cations.

The Fe^{v3+}(B) site with a hyperfine field of ~470 kOe arises when a diamagnetic cation, e.g. Mg^{2+}, is among the nearest neighbors to Fe^{3+}(A). When the charge in the tetrahedral cation sublattice decreases, e.g. $Fe^{3+} \rightarrow Mg^{2+}$, the nearest neighboring oxygen ions become electron deficient. Consequently, to ensure the electroneutrality, the charge in the octahedral cation sublattice increases, i.e. $Fe^{2.5+}$(B) $\rightarrow$ Fe^{v3+}(B), with the transfer of a valence electron to oxygen ions. The loss of one magnetic coupling of the octahedral cation with tetrahedral cations leads to a decrease in the hyperfine field from 495 kOe for Fe^{3+}(A + B) of stoichiometric magnetite to 470 kOe for Fe^{v3+}(B) (Table 2, Fig. 7b).

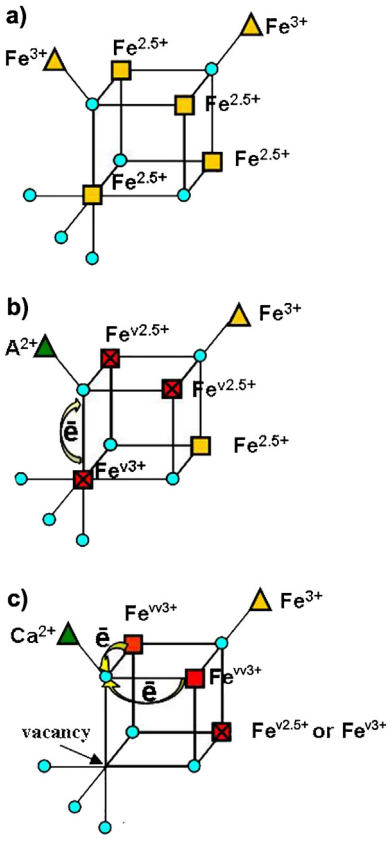

Fig. 7. Schematic fragment of the spinel structure. ○ is the oxygen, □ is the octahedral and △ is the tetrahedral cations; a) positions of iron in stoichiometric magnetite; b) the emergence of tetrahedral A^{2+}-cation causes positions Fe^{v3+} and $Fe^{v2.5+}$; c) the emergence of Ca^{2+} and cation vacancy leads to the formation of positions Fe^{vv3+} and $Fe^{v2.5+}$.

The $Fe^{2.5+}$ sites of stoichiometric magnetite transform into the $Fe^{v2.5+}$ sites due to the presence of the nearest diamagnetic tetrahedral A^{2+}-cation. Owing to the loss of one magnetic coupling with the tetrahedral sublattice, the hyperfine field decreases from 460 to 426 kOe. Upon inclusion of the large Ca^{2+} cation with an ionic radius of 1.04 Å into a tetrahedral site, a cation vacancy is formed in the close vicinity to this cation, thus creating local distortions and charge gradient in the lattice. The co-existence of these two defects among the neighbors of the octahedral B-cation leads to the formation of the Fe^{vv3+}(B) site with the hyperfine field of 400 kOe (Fig. 7c, Table 2). These sites were formed from the $Fe^{2.5+}$(B) sites of stoichiometric magnetite and dropped out of the process of fast electron exchange upon localization of the cation valence electron at the oxygen ion.

It should be noted that the sites Fe^{v3+}(B) and $Fe^{v2.5+}$(B) are typical for ferrospheres of the B(n) series with the total iron content of 76–79 wt% (Table S1, supplementary data), whereas the Fe^{vv3+}(B) sites were identified only in the ferrospheres with high-iron content of the S(n) and SMF(n) series (Fig. 8, Table 1). Their concentration was significantly increased after the OCM reaction over ferrospheres with overall content of $Fe_2O_3 \geq 89$ wt%.

The fraction of iron in ferrite spinel and hematite phases significantly depends on the iron concentration in ferrospheres (Fig. 9). For the as-received samples with $Fe_2O_3 \geq 89$ wt% under consideration of all iron sites, the content of the ferrite spinel phase decreases, whereas the content of the hematite phase increases with increasing overall content of Fe_2O_3 (Fig. 9a). The phase changes became even more pronounced after the OCM reaction on ferrospheres. In

Table 2
Iron positions in spinel phase of ferrospheres identifiable by Mössbauer method.

Fe position	*IS*, mm/s	*H*, kOe	The local environment of position
Fe^{3+}(A + B)	0.27 ± 0.04	495 ± 6	Stoichiometric magnetite
$Fe^{2.5+}$(B)	0.64 ± 0.04	460 ± 3	Stoichiometric magnetite, fast electronic exchange
Fe^{v3+}(B)	0.43 ± 0.04	470 ± 3	Diamagnetic A^{2+}-neighbor, localization of the electron on the oxygen
$Fe^{v2.5+}$(B)	0.65 ± 0.07	426 ± 8	Diamagnetic A^{2+}-neighbor, fast electronic exchange
Fe^{vv3+}(B)	0.37 ± 0.13	400 ± 20	Ca^{2+}(A)-neighbor + cation vacancy, localization of the electron on the oxygen

IS is isomer chemical shift relative to αFe, *H* is hyperfine magnetic field on Fe nuclei.

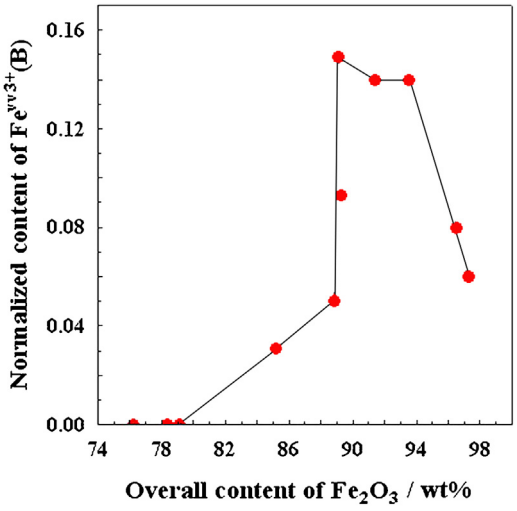

Fig. 8. The dependence of content of Fe^{3vv+}(B) positions on the overall iron content in steady state ferrospheres.

this case, ferrospheres of the series S(n) and SMF(n) underwent stronger changes than those of the B(n) series.

It is important to mention that both Mössbauer (Fig. 9) and XRPD (Fig. 4) studies revealed very similar relationships between the phase composition of ferrospheres and overall Fe_2O_3 content. Such good agreement between these two characterization methods allows us to conclude that our analysis of Mössbauer spectra adequately describes the defect states of the spinel structures ($Fe^{v2.5+}$(B), Fe^{v3+}(B), Fe^{vv3+}(B)) which can be involved as the active sites of the OCM process.

3.3. Nature of the active centers of oxidative coupling of methane

On the basis of the results of catalytic tests, XRPD and Mössbauer characterization together with relevant literature data, the below discussion is aimed at identifying OCM selective (formation of C_2-hydrocarbons) and non-selective (CO_x formation) phases/sites in ferrospheres. Iron species in such materials are located in three main iron-containing phases: ferrospinel, hematite, and alumosilicate glass. It is well established that oxide AB_2O_4 systems with the spinel structure are effective catalysts for deep oxidation of methane in excess oxygen [32–35]. Their activity is determined by the oxygen binding energy, which is mainly affected by the cations Cr^{3+}, Co^{3+}, and Fe^{3+} in the octahedral sites of the spinel, whereas the properties of divalent cations in the tetrahedral environment play a secondary role. For the aforementioned ions, the $Fe^{3+}-O$ bond is the most stable thus making ferrites the least active deep oxidation catalysts among other spinel structures [32,36]. It is worth mentioning that pure Fe_2O_3 is significantly more active than the spinel structures [34]. Taking this literature data into account, we can safely conclude that the low yield of CO_2 over the ferrospheres with the overall content of $Fe_2O_3 \geq 89$ wt% (Fig. 2) does not correlate with the presence of α-Fe_2O_3 phase (Figs. 4 b, 9 b). Contrarily, we have observed a linear dependence of this yield on the population of

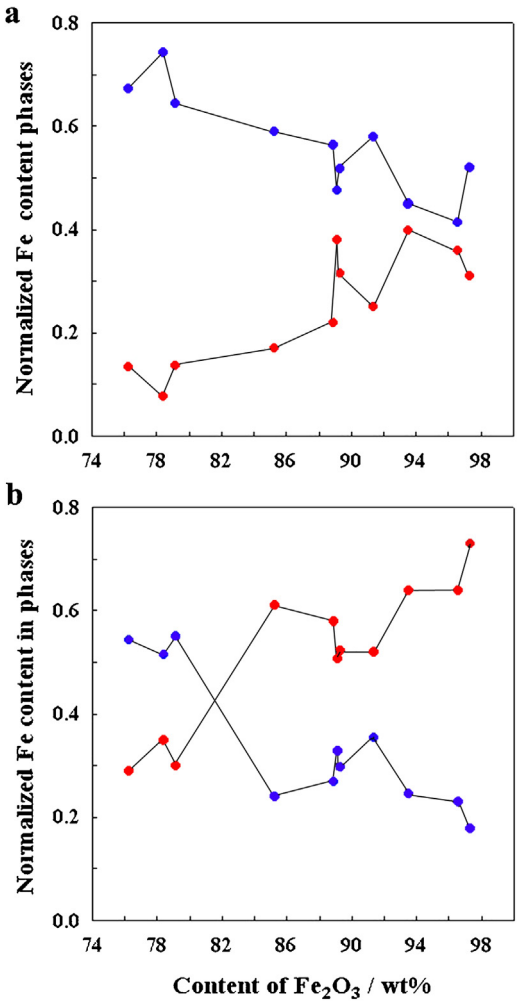

Fig. 9. Phases distribution of Fe in ferrospinel (●), hematite (●) in a) initial and b) steady states at 750 °C on the overall Fe_2O_3 content in ferrospheres.

iron sites located in the ferrospinel phase with the correlation coefficient of 0.95 (Fig. S2, supplementary data). According to [32,34,36] we also suggest that the activity of ferrospheres in methane oxidation to CO_2 is determined by the binding energy of the nucleophilic lattice oxygen in the spinel phase of the ferrospheres. However, what are the active sites for selective methane oxidation to C_2-hydrocarbons?

Different aspects of the influence of structural defects of single-phase and multiphase oxide systems on their OCM performance have been widely discussed in literature.[2,4–6,37–42] It is generally accepted that the OCM reaction is initiated by activation of methane on a surface oxygen species to yield gas-phase $CH_3^{\bullet}$ radicals recombining further to C_2H_6. The importance of electrophilic oxygen species such as O_2^{2-}, O^- in the OCM reaction has been highlighted in several studies. Their formation occurs through different mechanisms depending on the type of defect centers in the cat-

alytic system. In particular, high activity of Li/MgO catalysts was ascribed to the presence of [LiO^-] defect sites, which are responsible for the activation of methane with formation of CH_3 radical [2,4–6,39]. Structural oxygen vacancies in La_2O_3, Sm_2O_3, Nd_2O_3 and promoted M/La_2O_3 or Sm_2O_3 (M = Ca, Sr, Ba) oxides were suggested to influence the OCM activity; their concentration can be increased by promoting host oxides with metal oxides of lower oxidation state [5,38,42].

In addition, structural ordering of oxygen vacancies in metal oxide catalysts positively influence on their OCM performance. For example, tetragonal $Sr_{0.8}Gd_{0.2}CoO_{3-\delta}$ perovskites with ordered oxygen vacancies and Gd^{3+}/Sr^{2+} ions were about five times less active in total methane combustion at 500 °C, but showed four times higher selectivity to C_2-hydrocarbons at 850 °C than their cubic-phase counterparts with randomly distributed oxygen vacancies [43]. A similar difference in the structure of oxygen vacancies was also observed for two phases of Sm_2O_3. Such vacancies are distributed randomly in the monoclinic Sm_2O_3, while ordered pairs of anion vacancies are stabilized in the cubic Sm_2O_3 [44]. According to [45] the cubic phase was eight times more active in the formation of C_2H_6 at 600 °C compared to the monoclinic phase. Thus, it can be concluded that the mechanisms of oxygen activation on this two systems are in many aspects similar and include the oxygen adsorption on ordered oxygen vacancies. Electron required for this process is supplied by host ion oxidation for reducible complex oxides and by impure ion oxidation for irreducible simple oxides. In both cases, electrophilic oxygen species are formed.

The closest analog to the studied ferrospheres in the structure and properties of catalytically active phase is $ZnFe_2O_4$ with the cubic lattice parameter $a = 8.442$ Å. In the reaction medium $CH_4:O_2:Ar = 41.6:8.4:50$ vol% at 750 and 825 °C, it provides the yields of C_2-hydrocarbons about 3 and 13%, respectively [46], which are slightly higher than the values for the ferrospheres. As in the case of Ca-ferrospinel, the cation Zn^{2+} with the ionic radius of 0.6 Å occupies the tetrahedral positions. Unfortunately, the phase composition and the state of iron after the catalytic reaction were not studied. It was only observed, that at temperatures above 825 °C a collapse of the crystalline structure occurred due to the sublimation of ZnO.

For the iron-containing catalysts $Ca(Sr,Ba)_{0.5}La_{1.5}Fe_{0.5}Li_{0.5}O_4$ and $SrLaFe_{0.5}Zn(Mg)_{0.5}O_4$ with the K_2NiF_4 structure, a correlation between the yield of C_2-hydrocarbons and the content of Fe^{4+} ions identified by Mössbauer spectroscopy was established [40]. It was suggested that the formation of electrophilic O^- occurred according to the scheme: $Fe^{4+} + O^{2-} \leftrightarrow Fe^{3+} + O^-$. Importantly, when iron ions were replaced by zinc or magnesium ions in the $SrLaFe_{0.5}Zn(Mg)_{0.5}O_4$ system, the Fe^{4+} concentration and the yield of C_2-hydrocarbons increased [40].

In contrast to the catalysts with the K_2NiF_4 structure possessing Fe^{4+}, a defective Fe^{vv3+} state was formed upon incorporation of Ca^{2+} ions into the tetrahedral sites of the spinel structure in ferrospheres with high iron content. The concentration of such sites significantly increased with the total content of $Fe_2O_3 \geq 89$ wt% (Fig. 8). It is important to highlight that we were able to establish a linear dependence between the yield of C_2-hydrocarbons and the concentration of Fe^{vv3+}(B) sites with the correlation coefficient of 0.91 (Fig. 10). This relationship strongly suggests that Fe^{vv3+}(B) participate in the stabilization of oxygen species that are active and selective in the OCM reaction. The formation of such oxygen species and their participation in CH_4 activation can be illustrated as follows. As concluded from our characterization analysis, the inclusion of Ca^{2+} ion with a large ionic radius (1.04 Å) into the spinel structure stimulates the formation of a cation vacancy and an active center (Fig. 7c), which can be represented by [Fe^{vv3+}–O^{2-}–vac]. As a result, oxygen ions in the vicinity of this defect have a substantial

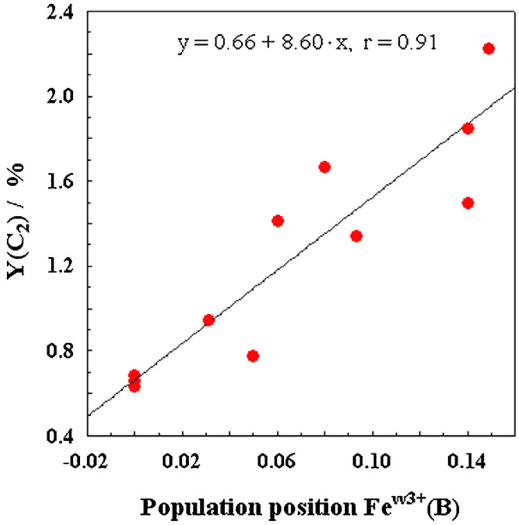

Fig. 10. The dependence of C_2-hydrocarbons yield at 750 °C on Fe^{vv3+}(B) population position.

deficiency of electrons. This deficiency is compensated by neighboring iron cations. The formed center [Fe^{vv3+}–O^{2-}–vac] increases the Madelung lattice energy due to the creation of a charge gradient and tends to return to the ground state at any opportunity. In conventional iron oxide compounds, the energy of ligand–cation electron excitation lies in the range from four to six eV [47]. Oxygen species in such center becomes apparently electrophilic in the presence of methane that is essential for homolytic breaking of the C—H bond to yield methyl radicals recombining to ethane (Eq. (1)). Fe^{vv3+} is reduced to Fe^{vv2+} upon CH_4 activation. Summarizing the above discussion, the ethane formation in the OCM reaction can be represented in the form of reduction and re-oxidation steps of the active sites:

$$4[Fe^{vv3+} - O^{2-} - vac] + 4CH_4 \rightarrow 4[Fe^{vv2+} - OH - vac] + 2C_2H_6 \quad (1)$$

$$4[Fe^{vv2+} - OH - vac] + 2O_2 \rightarrow 4[Fe^{vv3+} - O^{2-} - vac] + 2H_2O \quad (2)$$

The interaction of methane with electrophilic oxygen leads to the reduction of active center and the formation of the methyl radical. Ethane is formed by further recombination of CH_3 radicals in the gas phase (Eq. (1)). A re-oxidation of the reduced iron species by the gas-phase oxygen leads to a simultaneous formation of the initial active center and water (Eq. (2)).

Thus, we demonstrate that the type of defect iron species determines the OCM performance of ferrospheres in crystalline phases. The stabilization of certain defect/phase depends on the overall Fe_2O_3 content and the presence of Ca^{2+} dopants in the lattice of ferrite spinel. The derived knowledge may be used for designing OCM catalysts with improved performance.

4. Conclusions

The results of catalytic tests and catalysts characterization by XRPD analysis and Mössbauer spectroscopy enabled us i) to derive molecular insights into the states and distributions of iron cations in ferrospheres with Fe_2O_3 content in the range from 76 to 97 wt% and ii) to explain their effect on selectivity in the oxidative coupling of methane. The main identified phases were the ferrite spinel and hematite, with their concentration decreasing and increasing with the overall iron content, respectively. The spinel phase of ferrospheres with Fe_2O_3 content <89 wt% is magnetite diluted by diamagnetic cations. A liner correlation between the iron fraction in this phase and CO_2 yield was established, thus indicating that its nucleophilic lattice oxygen participates in the deep oxi-

dation of methane. Contrarily, electrophilic oxygen species in the spinel phase of ferrospheres with higher Fe_2O_3 content are selective for the methane oxidation to C_2-hydrocarbons. Such species are formed upon incorporation of Ca^{2+} ions into the tetrahedral sites of the spinel structure with simultaneous generation of an octahedral cation vacancy in the nearest neighborhood.

Acknowledgments

This study was supported by the Russian Science Foundation (project no. 14-13-00289).

Appendix A. Supplementary data

Supplementary data associated with this article can be found, in the online version, at http://dx.doi.org/10.1016/j.apcata.2016.06.032.

References

[1] G.E. Keller, M.M. Bhasin, J. Catal. 73 (1982) 9–19.
[2] T. Ito, J.H. Lunsford, Nature 314 (1985) 721–722.
[3] J.S. Lee, S.T. Oyama, Catal. Rev.–Sci. Eng. 30 (1988) 249–280.
[4] J.H. Lunsford, Angew. Chem. Int. Edit. 34 (1995) 970–980.
[5] E.N. Voskresenskaya, V.G. Roguleva, A.G. Anshits, Catal. Rev. −Sci. Eng. 37 (1995) 101–143.
[6] E.V. Kondratenko, M. Baerns, Handbook of Heterogeneous Catalysis, in: H. Ertl, F. Knozinger, J. Weitkamp (Eds.), Wiley-VCH Verlag GmbH & Co. KGaA, Weinheim, 2008, pp. 3010–3023.
[7] U. Zavyalova, M. Holena, R. Schlögl, M. Baerns, ChemCatChem 3 (2011) 1935–1947.
[8] C. Hammond, S. Conrad, I. Hermans, ChemSusChem 5 (2012) 1668–1686.
[9] P. Tang, Q. Zhu, Z. Wu, D. Ma, Energy Environ. Sci. 7 (2014) 2580–2591.
[10] Y.S. Su, J.Y. Ying, W.H. Green Jr., J. Catal. 218 (2003) 321–333.
[11] J. Labinger, Catal. Lett. 1 (1988) 371–375.
[12] A.G. Anshits, E.N. Voskresenskaya, E.V. Kondratenko, E.V. Fomenko, E.V. Sokol, Catal. Today 42 (1998) 197–203.
[13] E.V. Fomenko, E.V. Kondratenko, O.M. Sharonova, V.P. Plekhanov, S.V. Koshcheev, A.I. Boronin, A.N. Salanov, O.A. Bajukov, A.G. Anshits, Catal. Today 42 (1998) 273–277.
[14] A.G. Anshits, E.V. Kondratenko, E.V. Fomenko, A.M. Kovalev, O.A. Bajukov, N.N. Anshits, E.V. Sokol, D.I. Kochubey, A.I. Boronin, A.N. Salanov, S.V. Koshcheev, J. Mol. Catal. A: Chem. 158 (2000) 209–214.
[15] A.G. Anshits, E.V. Kondratenko, E.V. Fomenko, A.M. Kovalev, N.N. Anshits, O.A. Bajukov, E.V. Sokol, A.N. Salanov, Catal. Today 64 (2001) 59–67.
[16] O.M. Sharonova, N.N. Anshits, L.A. Solovyov, A.N. Salanov, A.G. Anshits, Fuel 111 (2013) 332–343.
[17] O.M. Sharonova, N.N. Anshits, A.G. Anshits, Inorg. Mater. 49 (2013) 586–594.
[18] S.N. Vereshchagin, E.V. Kondratenko, E.V. Rabchevskii, N.N. Anshits, L.A. Solov'ev, A.G. Anshits, Kinet. Catal. 53 (2012) 449–455.
[19] H.M. Rietveld, J. Appl. Cryst. 2 (1969) 65–71.
[20] L.A. Solovyov, J. Appl. Cryst. 37 (2004) 743–749.
[21] N.N. Anshits, O.A. Bayukov, E.V. Eremin, L.A. Solov'ev, E.V. Rabchevskiĭ, A.G. Anshits, Phys. Solid State 52 (2010) 1188–1192.
[22] O.A. Bajukov, N.N. Anshits, M.I. Petrov, A.D. Balaev, A.G. Anshits, Mater. Chem. Phys. 114 (2009) 495–503.
[23] W. Kündig, H. Bömmel, G. Constabaris, R.H. Lindquist, Phys. Rev. 142 (1966) 327–333.
[24] J.M. Daniels, A. Rosencwaig, J. Phys. Chem. Solids 30 (1969) 1561–1571.
[25] C. Wynter, T.M. Clark, B.J. Evans, M.A. Edwards, D. Radcliffe, J.A. Hall, Hyperfine Interact. 112 (1998) 231–234.
[26] A. Ito, K. Ôno, Y. Ishikawa, J. Phys. Soc. Jpn. 18 (1963) 1465–1473.
[27] R.J. Armstrong, A.H. Morrish, G.A. Sawatzky, Phys. Lett. 23 (1966) 414–416.
[28] J. de Sitter, A. Govaert, E. de Grave, D. Chambaere, G. Robbrecht, Phys. Status Solidi A 43 (1977) 619–624.
[29] R. Geírardin, A. Bonazebi, E. Millon, J.F. Brice, O. Evrard, J.P. Sanchez, J. Solid State Chem. 78 (1989) 154–163.
[30] J. Cieslak, S.M. Dubiel, J. Orewczyk, S. Jasienska, J. Phys. IV (07) (1997), C1-589–C1-590.
[31] S. Krupicka, Physik Der Ferrite Und Der Verwandten Magnetischen Oxide, ACADEMIA, Prague, 1973.
[32] G.K. Boreskov, V.V. Popovskii, V.A. Sazonov, Basis the catalytic action fore sight, in: Proceedings of the IV International Congress on Catalysis, Nauka Moscow, 1970, pp. 343–354.
[33] T.V. Andrushkevitch, G.K. Boreskov, V.V. Popovskii, V.S. Muzykantov, O.N. Kimkhai, V.A. Sazonov, Kinet. Katal. 9 (1968) 595–604 (in Russian).
[34] G.K. Boreskov, V.V. Popovskii, N.E. Lebedeva, V.A. Sazonov, T.V. Andrushkevitch, Kinet. Katal. 11 (1970) 1253–1261 (in Russian).
[35] V. Popovskii, G.K. Boreskov, Z. Dzevensky, V.S. Muzykantov, T.T. Shulmeister, Kinet. Katal. 12 (1971) 979–984 (in Russian).
[36] G.K. Boreskov, Catalysis The Questions of Theory and Practice, Nauka, Novosibirsk, 1987 (in Russian).
[37] N.G. Maksimov, G.E. Selyutin, A.G. Anshits, E.V. Kondratenko, V.G. Roguleva, Catal. Today 42 (1998) 279–281.
[38] A.G. Anshits, E.N. Voskresenskaya, L.I. Kurteeva, Catal. Lett. 6 (1990) 67–75.
[39] S. Arndt, G. Laugel, S. Levchenko, R. Horn, M. Baerns, M. Scheffler, R. Schlögl, R. Schomäcker, Catal. Rev. −Sci. Eng. 53 (2011) 424–514.
[40] Q. Yan, Y. Jin, Y. Wang, Y. Chen, X. Fu, Proc 10th Int. Congr. Catal., Budapest, Hungary, 1992, pp. 2230–2232.
[41] A. Burrows, C.J. Kiely, G.J. Hutchings, R.W. Joyner, M.Y. Sinev, J. Catal. 167 (1997) 77–91.
[42] J.M. Deboy, R.F. Hicks, J. Catal. 113 (1988) 517–524.
[43] S.N. Vereshchagin, L.A. Solovyov, E.V. Rabchevskii, V.A. Dudnikov, S.G. Ovchinnikov, A.G. Anshits, Chem. Commun. 50 (2014) 6112–6115.
[44] A.F. Wells, Structural Inorganic Chemistry, Oxford University Press, Oxford, 1984.
[45] K.P. Peil, G. Marcelin, J.G. Goodwin Jr, Methane conversion by oxidative processes methane, in: E.E. Wolf (Ed.), Fundamental and Engineering Aspects, Springer, The Netherlands, 1992, pp. 138–167.
[46] F. Papa, L. Patron, O. Carp, C. Paraschiv, B. Ioan, J. Mol. Catal. A: Chem. 299 (2009) 93–97.
[47] O.A. Bayukov, A.F. Savitskii, Phys. Status Solidi B 155 (1989) 249–255.